Article:

Dissanayake, DMMP, Zhou, C, Poologanathan, K et al. (3 more authors) (2021) Numerical Simulation and Design of Stainless Steel Hollow Flange Beams under Shear. Journal of Constructional Steel Research, 176. 106414. ISSN 0143-974X

https://doi.org/10.1016/j.jcsr.2020.106414

Numerical Simulation and Design of Stainless Steel Hollow Flange Beams under Shear

D. M. M. P. Dissanayake
Faculty of Engineering and Environment, University of Northumbria, Newcastle, UK.
C. Zhou
Faculty of Engineering and Environment, University of Northumbria, Newcastle, UK.
K. Poologanathan
Faculty of Engineering and Environment, University of Northumbria, Newcastle, UK.
S. Gunalan
School of Engineering and Built Environment, Griffith University, Queensland, Australia.
K. D. Tsavdaridis
School of Civil Engineering, Faculty of Engineering and Physical Sciences, University of Leeds, UK.
J. Guss
Faculty of Engineering and Environment, University of Northumbria, Newcastle, UK.

Abstract

Stainless steel offers a range of benefits over conventional carbon steel in structural applications. This paper presents the detailed numerical modelling of shear response of cold-formed stainless steel hollow flange sections using finite element software package, Abaqus. The effect of geometric parameters such as section height and section thickness, and the influence of different steel grades were investigated following the validation of finite element models. From numerical results, the formation of diagonal tension fields can be clearly observed in the webs of rectangular hollow flange sections while more even distribution of the stresses in the webs is seen in triangular hollow flange sections. Further, a plastic hinge type mechanism is formed in triangular flanges at the post-failure region. The evaluation of

Eurocode 3 and the direct strength method shear design provisions for stainless steel hollow flange beams are found to be significantly conservative. Therefore, modified provisions were proposed and the comparison of those with finite element results confirmed the accurate and consistent shear resistance predictions over the codified provisions.

Keywords: Cold-formed stainless steel, Hollow flange sections, Finite element modelling, Shear, Eurocode 3, Direct strength method

1 Introduction

The increasing demand for stainless steel as a construction material can be seen over the other materials in the past few decades [1]. The key feature of stainless steel is its corrosion resistance making stainless steel structural components more durable while being recyclable material points out stainless steel as a sustainable solution to construction wastes. Even though, stainless steel costs approximately four times higher than conventional carbon steel, it is suggested in studies that stainless steel structures are more economical on the basis of whole life than carbon steel in aggressive conditions [2].

Cold-formed sections are more common among stainless steel sections compared to hot-rolled and built-up sections in light structural applications [3]. There are various types of cold-formed sections including open sections and hollow sections. The cross-sections of doubly symmetric rectangular hollow flange beams (RHFBs) and triangular hollow flange beams (THFBs) are shown in Fig. 1. These sections can be formed by connecting the cold-formed hollow flanges to the web elements using electric resistance welding. The doubly symmetric hollow flange sections are more stable to the torsional effects than the monosymmetric hollow flange channel sections, and closed flanges suppress the distortional buckling effects which are more likely to appear in open sections with free edges such as C-sections and Z-sections. Therefore, doubly symmetric hollow flange sections are comparable in stability to commercially available I-sections and are found to be structurally efficient than conventional cold-formed sections.

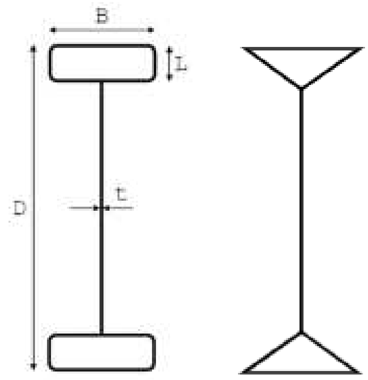

Fig. 1 Doubly symmetric hollow flange sections

A number of researches have investigated the structural behaviour of hollow flange sections in the past. Keerthan and Mahendran [4], [5] conducted experimental studies and numerical investigations on the shear behaviour of cold-formed steel rectangular hollow flange channel beams known as LiteSteel beams. Keerthan et al. [6], [7] investigated the combined bending and shear response of rectangular hollow flange channel sections using experimental and numerical studies. Moreover, both bending tests and numerical investigations have been conducted on the rivet-fastened rectangular hollow flange channel beams by Siahaan et al. [8], [9] while Wanniarachchi and Mahendran [10] experimented screw-fastened RHFBs to find out section moment capacities. Also, the structural behaviour of cold-formed channel sections has been thoroughly investigated by many researchers. Both experimental and numerical investigations on cold-formed steel channel sections have been conducted by Pham and Hancock [11]–[13] to study the combined bending and shear behaviour. The shear response of lipped channel sections has been studied by Keerthan and Mahendran [14] for cold-formed steel and Dissanayake et al. [15] for cold-formed stainless steel. In addition, the structural response of I-sections has been investigated by a number of studies over the years. Olsson [16] and Real et al. [17] performed shear tests on stainless steel plate girders while the bending and shear interaction behaviour of stainless steel plate girders has been investigated by Saliba and Gardner [18]. Further, the numerical investigations on lateral-torsional buckling behaviour of stainless steel I-sections have been carried out by Saadat and Ashraf [19]. However, research into cold-formed stainless steel hollow flange sections are relatively scarce.

The attention has been also given to the elastic shear buckling response of cold-formed sections by a number of researches [20]–[22]. Keerthan and Mahendran [22] conducted shear buckling analyses of different cold-formed sections including open and hollow flange beams using numerical modelling. They proposed a generalised equation to calculate the shear buckling coefficients of cold-formed sections. The proposed equation takes into account the level of fixity of the web-to-flange juncture. It was suggested from the findings that the level of fixity at the web-to-flange juncture of RHFBs and THFBs is closer to fixed support conditions by Keerthan and Mahendran [22].

The direct strength method (DSM) has been adopted in the current North American specifications, AISI S100 [23] and Australian and New Zealand standards, AS/NZS 4600 [24] for the design of cold-formed steel sections. The DSM considers the whole section buckling when determining the section resistance, therefore, takes into account the element interaction in the design calculations. However, the current European standards for cold-formed steel, EN19931-3 [25] and for stainless steel, EN1993-1-4 [26] do not take into account the beneficial element interaction that present at the web-to-flange juncture [27]. Therefore, it is expected to provide conservative resistance predictions from European standards for hollow flange sections.

In this paper, the shear response of cold-formed stainless steel hollow flange sections (RHFBs and THFBs) is discussed. The details of numerical modelling conducted to investigate the shear response of RHFBs and THFBs and the use of numerical results in the evaluation of codified design provisions are presented.

2 Finite element (FE) modelling

The numerical studies were conducted using commercially available FE software package ABAQUS CAE 2017 to investigate the shear response of cold-formed stainless steel hollow flange sections. The three-point loading setup used by Keerthan and Mahendran [4] in the shear tests of single LiteSteel beams were incorporated in the development of FE models. The details of numerical modelling and model validation are given in this section.

2.1 Development of FE model

In each FE model, single hollow flange sections were modelled together with three web side plates (WSPs) placed at the supports and at the loading point to simulate three-point loading tests. The quadrilateral four-node shell element with reduced integration, S4R was picked from the element library for the modelling of hollow flange sections. A 5 mm × 5 mm mesh was assigned for the flat parts of the sections while employing a relatively finer mesh of 1 mm × 5 mm to the corner regions following the mesh sensitivity analyses. The rigid quadrilateral element with four nodes, R3D4 was chosen to simulate the WSPs which have a relatively higher stiffness. The centre point of each plate was assigned as the rigid body reference point to which the motion of the rigid plates was then coupled. A 10 mm × 10 mm mesh was assigned to WSPs. Fig. 2 shows the different parts of the FE model and FE mesh.

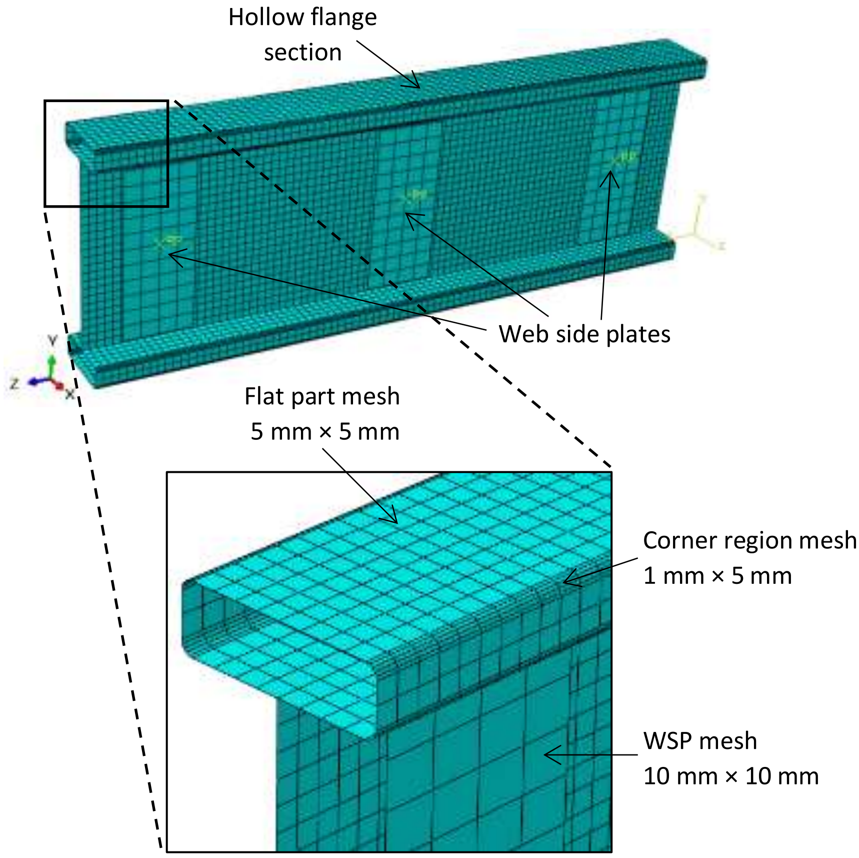

Fig. 2 Assembly of parts and FE mesh used in the modelling

In this study, recent proposals suggested by Arrayago et al. [28] to two-stage Ramberg-Osgood material model were incorporated to represent the non-linear material response of stainless steel while an elastic, perfectly-plastic material model was employed to model carbon steel behaviour in FE models. Then, stress-strain material data was fed into Abaqus in the form of true stress (σ_{true}) and log plastic strain (ε_{ln}^{pl}). As a result of cold-work of forming, material properties of corner regions of stainless steel cross-sections are enhanced. A number of studies have investigated these strength enhancements and predictive models have been proposed [29]–[31]. These induced strengths in corner regions were explicitly considered in the numerical modelling and the more details of this can be found in [15]. The effects of residual stresses were not incorporated in the numerical modelling of this study and were found to be negligible from similar numerical studies [5], [32], [33].

In the three-point loading tests, WSPs were attached to the section webs to eliminate any bearing failure that could occur at the supports or at the loading point. Therefore, in the FE models, boundary conditions and loading were assigned to the WSPs through the coupled rigid body reference points. Pin support conditions were employed at the two beam ends to maintain simply supported conditions. The in-plane translational DOFs of the cross-sectional plane (x-y plane) were restrained for the application of pin supports to the beam sections and the rotational DOF about the longitudinal axis (z-axis) of the section was restrained to avoid possible torsional effects. At the mid-span WSP, a downward displacement was applied to the reference point to simulate the loading of the section. The tie constraints available in Abaqus were employed to represent the bolted connections between section webs and WSPs. Fig. 3 illustrates the assigned boundary conditions in the FE modelling.

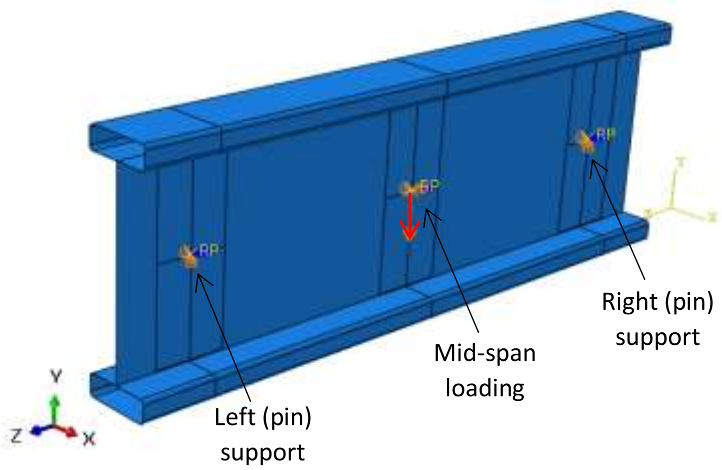

Fig. 3 Assigned boundary conditions in the FE modelling

The effects of the local geometric imperfections on the performance of thin steel section behaviour is required to be taken into account in the numerical analysis. The details of numerical modelling of geometric imperfections have been reviewed in previous studies [34]–[36]. To calculate the magnitude of the local geometric imperfections (ω_0) of steel sections, Gardner and Nethercot [34] proposed modifications to the original prediction model developed by Dawson and Walker [37]. This modified Dawson and Walker model was employed in this study to represent the magnitude of the local geometric imperfections. This model is given by Eq. (1).

$$\omega_0 = 0.023\left(\frac{\sigma_{0.2}}{\sigma_{cr}}\right)t \quad (1)$$

where $\sigma_{0.2}$ is the 0.2 % proof stress of the material, σ_{cr} is the critical elastic buckling stress of the most slender plate element of the section, and t is the cross-sectional thickness.

Two types of analysis were performed on each FE model. First, an Eigenvalue buckling analysis was conducted to identify the critical buckling modes of the structure. These critical modes were then introduced to the non-linear FE models to perturb the mesh to account for the initial geometric imperfection patterns. Then, a geometrically and materially non-linear analysis was performed on the FE models using a modified Static Riks analysis to investigate the failure mechanism and the post-buckling behaviour of the sections.

2.2 Model validation

The shear tests conducted by Keerthan and Mahendran [4] on cold-formed steel hollow flange channel sections (LiteSteel beams) were used for the validation. The compared hollow flange sections have a shear span to clear web depth ratio (aspect ratio) of 1.0 to govern shear failure in the sections. More details of the experiments can be found in [4].

The experimental and FE ultimate loads ($V_{Exp.}$ and V_{FE}) are compared in Table 1. From the comparisons, it can be seen that experimental shear resistance to FE shear resistance ratio has a mean of 0.99 and a coefficient of variation (COV) of 0.039. Therefore, it is clear that the numerical models are able to predict the ultimate shear capacities of the hollow flange sections accurately.

Table 1 Experimental [4] and FE shear resistances of LSBs

LSB section	$V_{Exp.}$ (kN)	V_{FE} (kN)	$V_{Exp.}/V_{FE}$
LSB 150×45×15×2.0	68.5	69.84	0.98
LSB 200×60×20×2.0	88.2	87.54	1.01
LSB 200×60×20×2.5	119.3	115.64	1.03
LSB 250×75×25×2.5	139.6	137.88	1.01
LSB 300×75×25×2.5	143.7	155.28	0.93
Mean			0.99
COV			0.039

The cross-section designation: *Section name Section depth (D)* × *Section breadth (B)* × *Flange height (L)* × *Thickness (t)* was used to denote the considered cross-sections in this study. For an instance, a rectangular hollow flange channel section (LiteSteel beam) with a depth of 150 mm, a breadth of 45 mm, a flange height of 15 mm and a thickness of 2.0 mm is denoted as *LSB 150×45×15×2.0*.

In addition, the failure mechanisms were compared to further assess the FE models with the experimental results. Fig. 4 illustrates the experimental and FE shear failure modes of *LSB 150×45×15×2.0* section and the comparison is found to be fairly similar. Therefore, it can be concluded that the FE models simulate the shear failure mechanism of hollow flange sections reasonably well.

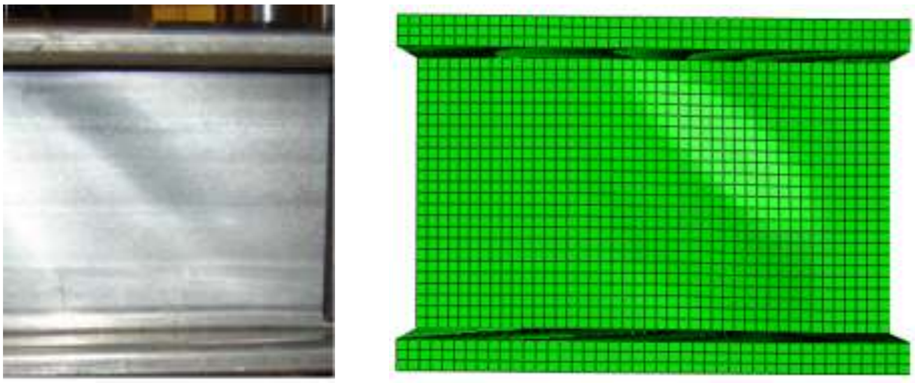

(a) (b)

Fig. 4 (a) Experimental [4] and (b) FE shear failure mechanisms of *LSB 150×45×15×2.0* section

3 Numerical parametric study

3.1 General

The influence of different cross-sectional dimensions and steel grades on the shear response of cold-formed stainless steel hollow flange sections were investigated utilising the validated numerical FE models. The shear response of RHFBs and THFBs were studied in this study. Two section heights (150 mm, 200 mm) and three section thicknesses (1 mm, 1.5 mm, 2 mm) were taken into account and four stainless steel grades including austenitic grades (1.4301, 1.4311) and duplex grades (1.4362, 1.4462) were considered in the study. In addition, more slender 250 mm and 300 mm deep RHFBs, and 250 mm deep THFBs, of 1 mm thick and of stainless steel grade 1.4462 were developed to have a wide range of FE data. Altogether, 51 FE models of stainless steel hollow flange beams were developed. The material properties for stainless steel grades were found from EN1993-1-4 [26]. Young's modulus and Poisson's ratio were taken as 200,000 MPa and 0.3, respectively. Sections with an aspect ratio of 1.0 were used to govern the shear response.

3.2 FE shear resistances of hollow flange sections

The FE shear capacities of RHFBs and THFBs are summarised in Tables 2 and 3. Further, the comparisons of FE shear resistances with EN19931-4 [26] and the DSM predictions, and the proposed predictions are also included in tables. The details of these codified shear design provisions and the details of new proposals are discussed in Section 4.

Table 2 Parametric study results with EN1993-1-4 [26] and the DSM predictions for RHFB sections

Section	Stainless steel grade – 1.4301					Stainless steel grade – 1.4311					Stainless steel grade – 1.4362					Stainless steel grade – 1.4462				
	V_{FE} (kN)	V_{FE}/V_{EC3}	$V_{FE}/V_{EC3,\ Proposed}$	V_{FE}/V_{DSM}	$V_{FE}/V_{DSM,\ Proposed}$	V_{FE} (kN)	V_{FE}/V_{EC3}	$V_{FE}/V_{EC3,\ Proposed}$	V_{FE}/V_{DSM}	$V_{FE}/V_{DSM,\ Proposed}$	V_{FE} (kN)	V_{FE}/V_{EC3}	$V_{FE}/V_{EC3,\ Proposed}$	V_{FE}/V_{DSM}	$V_{FE}/V_{DSM,\ Proposed}$	V_{FE} (kN)	V_{FE}/V_{EC3}	$V_{FE}/V_{EC3,\ Proposed}$	V_{FE}/V_{DSM}	$V_{FE}/V_{DSM,\ Proposed}$
RHFB 150×45×15×1.0	18.84	1.50	1.09	1.35	1.16	21.57	1.45	1.03	1.33	1.11	29.72	1.47	1.00	1.37	1.09	32.27	1.48	1.01	1.39	1.09
RHFB 150×45×15×1.5	30.15	1.31	1.02	1.21	1.02	36.29	1.32	1.01	1.16	1.03	52.22	1.36	1.01	1.22	1.05	57.18	1.38	1.01	1.24	1.06
RHFB 150×45×15×2.0	45.31	1.18	1.02	1.37	1.01	54.12	1.24	1.02	1.30	1.01	77.32	1.32	1.02	1.19	1.02	84.49	1.32	1.02	1.17	1.03
RHFB 200×60×20×1.0	21.71	1.53	1.05	1.42	1.14	27.13	1.63	1.10	1.53	1.19	33.54	1.50	0.98	1.42	1.05	36.71	1.53	1.00	1.45	1.06
RHFB 200×60×20×1.5	34.18	1.28	0.95	1.14	0.99	41.82	1.32	0.96	1.19	1.02	60.18	1.38	0.96	1.28	1.04	65.75	1.40	0.97	1.30	1.05
RHFB 200×60×20×2.0	53.08	1.30	1.01	1.20	1.01	63.82	1.30	1.00	1.15	1.01	91.39	1.34	0.99	1.20	1.03	99.82	1.35	0.99	1.22	1.04
RHFB 250×75×25×1.0																40.84	1.60	1.02	1.52	1.05
RHFB 300×120×20×1.0																45.05	1.66	1.02	1.57	1.00

Table 3 Parametric study results with EN1993-1-4 [26] and the DSM predictions for THFB sections

Section	Stainless steel grade – 1.4301					Stainless steel grade – 1.4311					Stainless steel grade – 1.4362					Stainless steel grade – 1.4462				
	V_{FE} (kN)	V_{FE}/V_{EC3}	$V_{FE}/V_{EC3,Proposed}$	V_{FE}/V_{DSM}	$V_{FE}/V_{DSM,Proposed}$	V_{FE} (kN)	V_{FE}/V_{EC3}	$V_{FE}/V_{EC3,Proposed}$	V_{FE}/V_{DSM}	$V_{FE}/V_{DSM,Proposed}$	V_{FE} (kN)	V_{FE}/V_{EC3}	$V_{FE}/V_{EC3,Proposed}$	V_{FE}/V_{DSM}	$V_{FE}/V_{DSM,Proposed}$	V_{FE} (kN)	V_{FE}/V_{EC3}	$V_{FE}/V_{EC3,Proposed}$	V_{FE}/V_{DSM}	$V_{FE}/V_{DSM,Proposed}$
THFB 150×45×15×1.0	20.32	1.61	1.00	1.39	1.00	24.98	1.68	1.01	1.47	1.01	36.74	1.81	1.02	1.61	1.02	39.95	1.83	1.01	1.64	1.01
THFB 150×45×15×1.5	34.30	1.49	1.00	1.38	1.00	41.44	1.50	0.99	1.32	0.99	59.85	1.56	0.99	1.34	0.98	65.74	1.59	0.99	1.37	0.99
THFB 150×45×15×2.0	50.11	1.31	1.03	1.51	1.01	59.77	1.37	0.99	1.43	0.99	85.21	1.45	0.97	1.31	0.97	93.54	1.47	0.97	1.30	0.97
THFB 200×60×20×1.0	25.02	1.76	1.01	1.56	1.01	30.99	1.86	1.02	1.66	1.02	45.19	2.02	1.02	1.82	1.02	49.19	2.05	1.02	1.85	1.02
THFB 200×60×20×1.5	42.15	1.57	1.00	1.34	1.00	51.56	1.62	1.01	1.40	1.01	74.88	1.72	1.01	1.52	1.00	82.10	1.75	1.01	1.55	1.01
THFB 200×60×20×2.0	61.11	1.49	1.01	1.38	1.00	73.68	1.50	0.99	1.32	0.99	106.36	1.56	0.99	1.34	0.98	117.09	1.59	0.99	1.37	0.99
THFB 250×75×25×1.0																56.66	2.22	1.00	2.01	1.00

3.3 Results discussion

The shear response of cold-formed stainless steel RHFB sections and THFB sections are discussed in this section using the generated numerical FE results in the parametric study. Fig. 5 illustrates the shear response of *RHFB 150×45×15×1.0* section of stainless steel grade 1.4301 with its load-deflection curve while Fig. 6 shows that of *RHFB 200×60×20×1.0* section of the same steel grade. From Figs. 5 and 6, it can be seen that the out-of-plane buckling of section webs approximately start at point 1 where a change in section stiffness can be observed from the load-deflection curves. Then, the progressive buckling of both section webs at the failure point and at the post-failure regime can be observed under the shear loading. Further, the formed diagonal tension bands of highly stressed regions are clearly visible in *RHFB 150×45×15×1.0* section as a result of the anchoring provided to the webs by the transverse web stiffeners and flanges. However, these tension fields are normalised over the section webs in *RHFB 200×60×20×1.0* section.

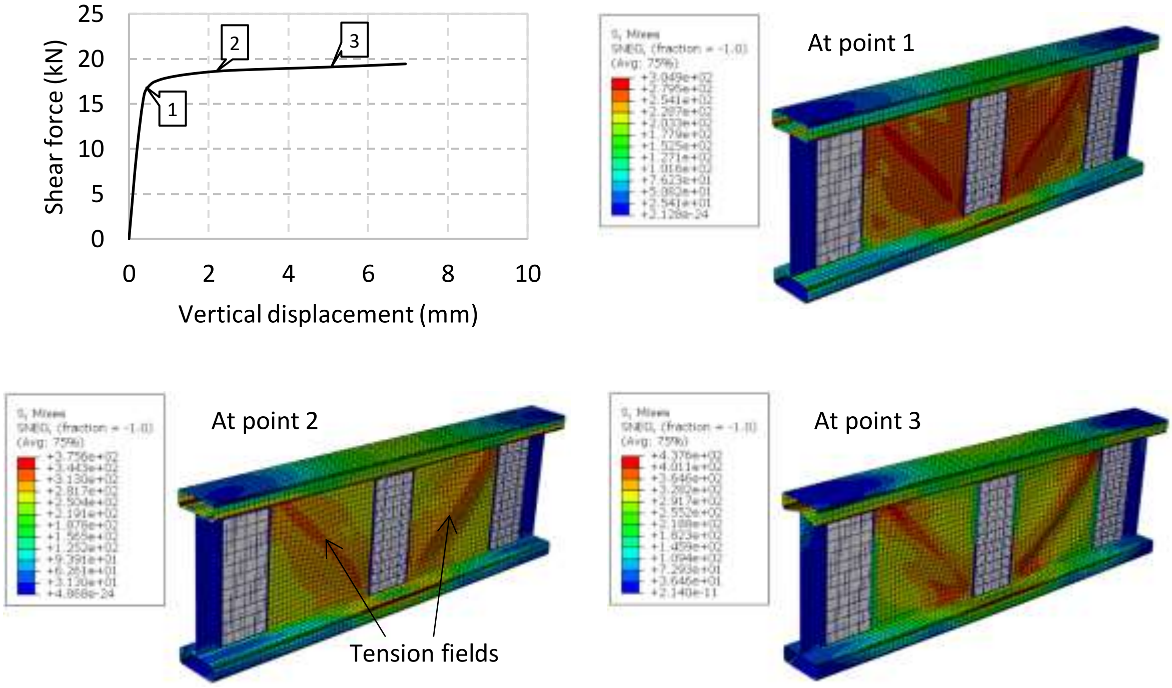

Fig. 5 Shear response of *RHFB 150×45×15×1.0* section at the different stages of load-deflection curve

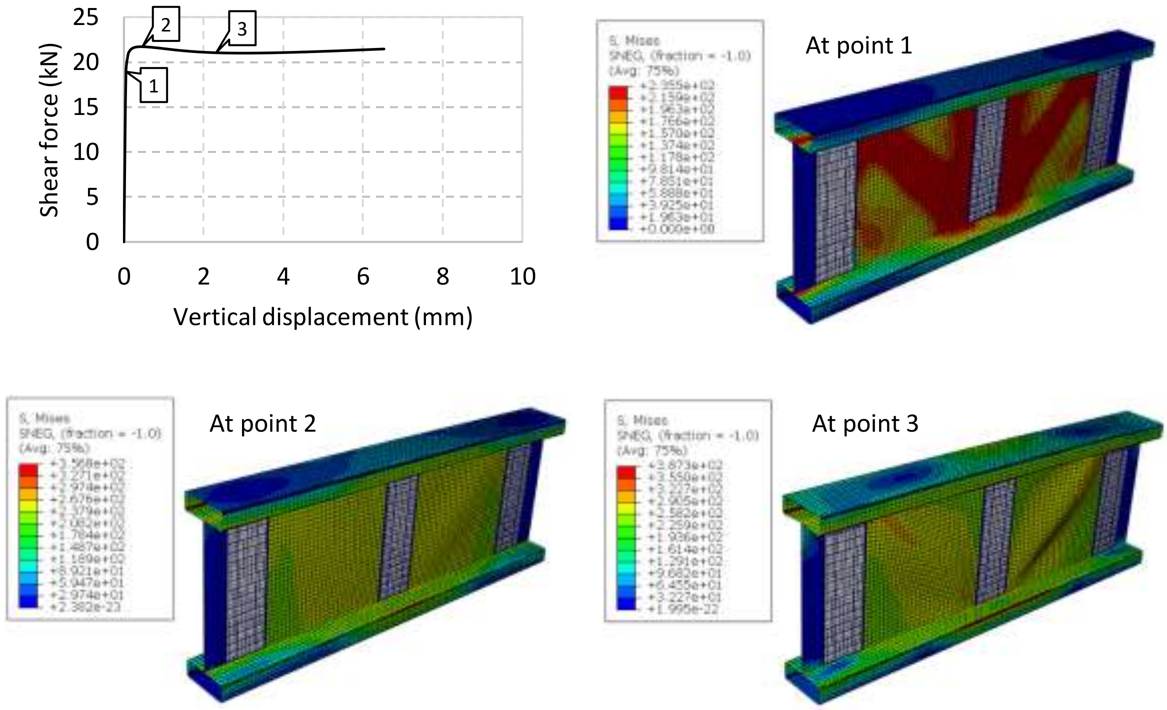

Fig. 6 Shear response of *RHFB 200×60×20×1.0* section at the different stages of load-deflection curve

Figs. 7 and 8 illustrate the shear behaviour of *THFB 150×45×15×1.0* section and *THFB 200×60×20×1.0* section of stainless steel grade 1.4301, respectively with their load-deflection curves. Both sections begin to show signs of out-of-plane buckling of webs at around point 1 of their load-deflection curves. After this, the progression of web shear buckling of both sections can be observed through their failure points. The increased anchoring facilitated by the triangular flanges and transverse web stiffeners caused the distribution of the stresses in the webs more evenly. Therefore, the diagonal tension bands are not clearly visible in THFB sections as opposed to RHFB sections. Moreover, a plastic hinge type mechanism is formed in the mid-span of THFB sections at the post-failure region. The excessive compression stresses induced within the triangular top flanges as a result of the anchoring provided by the top flanges to the tension fields could lead to this formation.

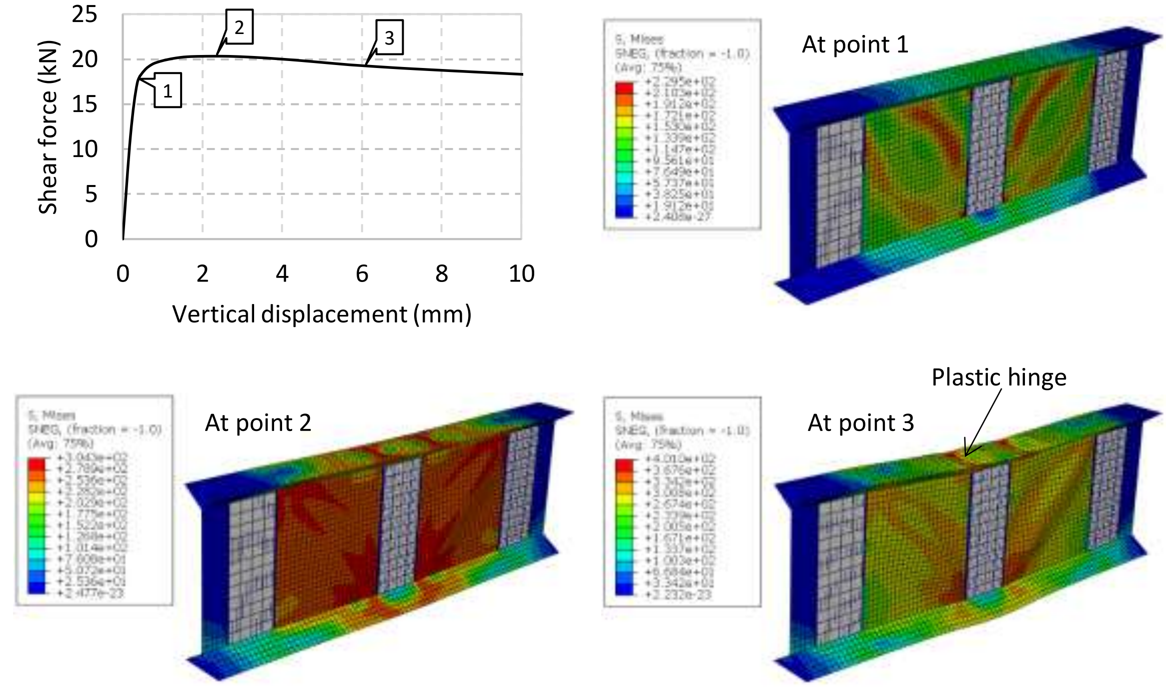

Fig. 7 Shear response of *THFB 150×45×15×1.0* section at the different stages of load-deflection curve

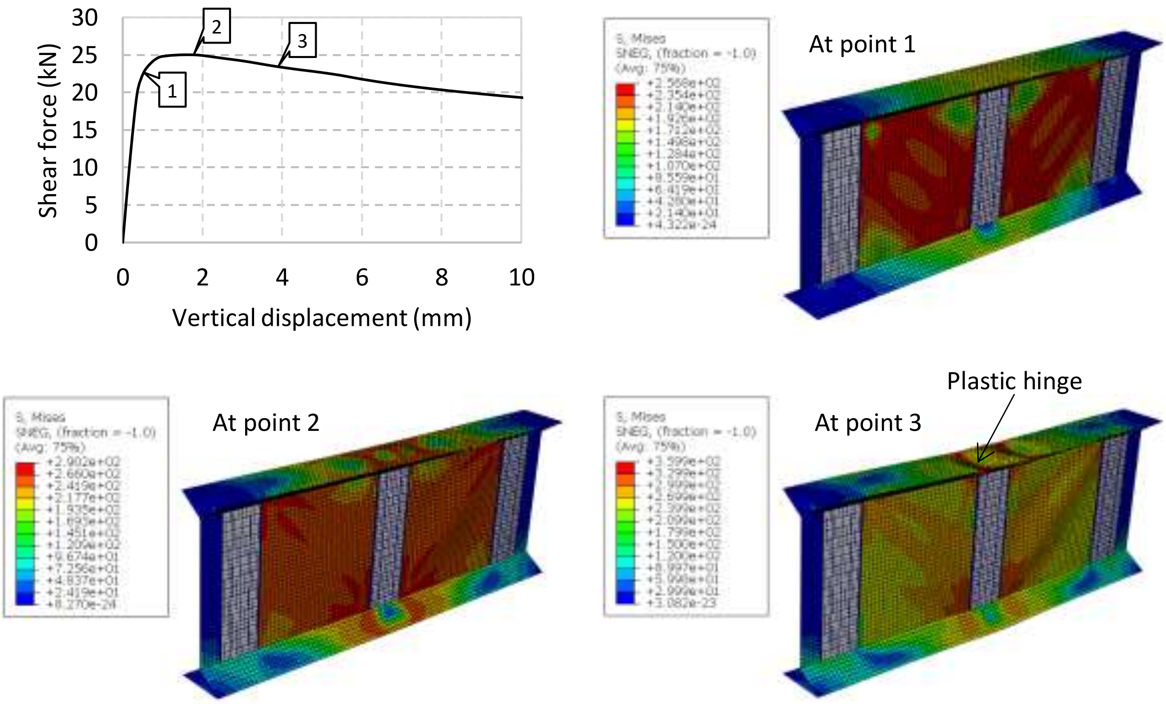

Fig. 8 Shear response of *THFB 200×60×20×1.0* section at the different stages of load-deflection curve

4 Assessment of shear design rules

The generated numerical database of hollow flange sections was incorporated in this section to evaluate the shear design rules provided in European standards for stainless steel [26] and the DSM shear design rules. Following the assessment of codified shear provisions, new shear design equations were proposed using FE results.

4.1 European standards for stainless steel, EN1993-1-4 [26]

European standards for stainless steel [26] adopts the shear design rules provided in European standards for plated steel, EN1993-1-5 [38]. According to that, the summation of the shear buckling resistance of the section web ($V_{bw,Rd}$) and the flange contribution to the shear resistance of the section ($V_{bf,Rd}$) gives the shear resistance of the section ($V_{b,Rd}$) as expressed in Eq. (2).

$$V_{b,Rd} = V_{bw,Rd} + V_{bf,Rd} \leq \frac{\eta f_{yw} h_w t_w}{\sqrt{3}\gamma_{M1}} \tag{2}$$

where the parameter η takes into account the strain hardening of stainless steel, γ_{M1} is the partial safety factor, f_{yw} is the yield strength of the web, h_w is the depth of the web, and t_w is the thickness of the web.

The shear buckling resistance of the web ($V_{bw,Rd}$) is given by Eq. (3) in which χ_w is the web shear buckling reduction factor.

$$V_{bw,Rd} = \frac{\chi_w f_{yw} h_w t_w}{\sqrt{3}\gamma_{M1}} \tag{3}$$

The flange contribution ($V_{bf,Rd}$) is defined by Eq. (4).

$$V_{bf,Rd} = \frac{b_f t_f^2 f_{yf}}{c\,\gamma_{M1}}\left(1 - \left(\frac{M_{Ed}}{M_{f,Rd}}\right)^2\right) \tag{4}$$

where b_f is the width of the flange, t_f is the thickness of the flange, and f_{yf} is the yield strength of the flange. M_{Ed} is the design bending moment of the section and $M_{f,Rd}$ is the moment resistance of the flanges alone. The parameter c is the distance to the location of the plastic hinge from the transverse stiffener. Eq. (5) is given in EN1993-1-4 [26] to calculate the parameter c.

$$c = a\left[0.17 + \frac{3.5\, b_f t_f^2 f_{yf}}{t_w h_w^2 f_{yw}}\right] \text{ and } \frac{c}{a} \leq 0.65 \tag{5}$$

where a is the length of the shear panel.

Two sets of expressions are set out in EN1993-1-4 [26] to calculate the web shear buckling reduction factor (χ_w) of the section webs with and without rigid end posts. These expressions for the webs with rigid end posts are given by Eqs. (6)-(8).

$$\chi_w = \eta \text{ for } \bar{\lambda}_w \leq 0.65/\eta \tag{6}$$

$$\chi_w = 0.65/\bar{\lambda}_w \text{ for } 0.65/\eta < \bar{\lambda}_w < 0.65 \tag{7}$$

$$\chi_w = 1.56/(0.91 + \bar{\lambda}_w) \text{ for } \bar{\lambda}_w \geq 0.65 \tag{8}$$

where $\bar{\lambda}_w$ is the slenderness of the web.

The EN1993-1-4 [26] shear design rules were then evaluated using the numerical FE results generated in Section 3 to assess their applicability to predict the shear resistance of cold-formed stainless steel hollow flange sections. The comparison of EN1993-1-4 [26] shear design rules with FE results for each section is given in Tables 2 and 3. The generated numerical shear capacities are plotted with EN1993-1-4 [26] web shear buckling reduction factor (χ_w) in Fig. 9 and can be seen that the codified shear provisions are too conservative for cold-formed stainless steel hollow flange sections. Further, THFBs are found to have higher shear resistances than RHFBs.

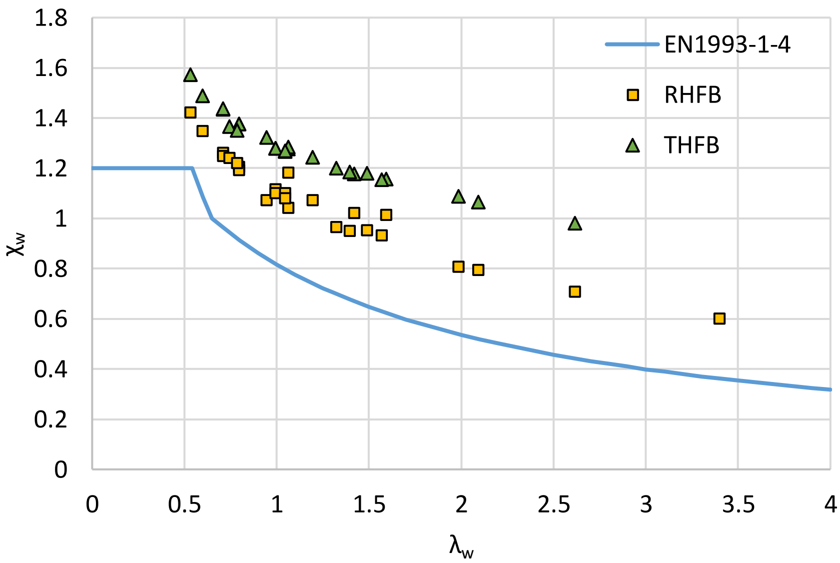

Fig. 9 Comparison of FE shear capacities with the web shear buckling reduction factor (χ_w) of EN1993-1-4 [26]

Table 4 summarises the overall mean and COV of FE shear resistance to predicted shear resistance ratio for each cross-section type. The conservative nature of EN1993-1-4 [26] shear capacity predictions for hollow flange sections is further confirmed from mean and COV values. Eurocode provisions do not take into account the favourable effect of fixity at the web-to-flange juncture of the hollow flange sections to shear buckling resistance of the section web could be one reason for these conservative predictions.

Table 4 Overall mean and COV of FE to predicted shear resistance ratio for each section type

	EN1993-1-4 [26]		DSM	
	Current	Proposed	Current	Proposed
RHFBs				
Mean	1.40	1.01	1.30	1.05
COV	0.087	0.034	0.097	0.048
THFBs				
Mean	1.66	1.00	1.49	1.00
COV	0.132	0.015	0.127	0.015

Therefore, Eurocode shear provisions were modified to enhance the shear resistance prediction accuracy of stainless steel hollow flange sections. The new set of expressions for web shear buckling reduction factor (χ_w) of EN1993-1-4 [26] were proposed using numerical FE shear capacities of hollow flange sections and following regression analyses. The elastic shear buckling coefficients proposed for RHFBs and THFBs by Keerthan and Mahendran [22] were utilised here when modifying the codified expressions. Therefore, proposed shear provisions do take into account the available fixity at the web-to-flange juncture.

The proposed expressions for web shear buckling reduction factor (χ_w) of RHFBs are given by Eqs. (9)-(11).

$$\chi_w = 1.4 \text{ for } \bar{\lambda}_w \le 0.5 \tag{9}$$

$$\chi_w = 1.08/\bar{\lambda}_w^{\;0.34} \text{ for } 0.5 < \bar{\lambda}_w < 1.25 \tag{10}$$

$$\chi_w = 2.75/(1.5 + \bar{\lambda}_w) \text{ for } \bar{\lambda}_w \ge 1.25 \tag{11}$$

Eqs. (12) and (13) provides the modified expressions for web shear buckling reduction factor (χ_w) of THFBs.

$$\chi_w = 1.53 \text{ for } \bar{\lambda}_w \le 0.5 \tag{12}$$

$$\chi_w = 1.245/\bar{\lambda}_w^{\;0.29} \text{ for } 0.5 < \bar{\lambda}_w \tag{13}$$

Fig. 10 plots the proposed expressions for web shear buckling reduction factor (χ_w) for stainless steel hollow flange sections with FE shear capacities. It can be seen that the proposed curves are fitted well with the distribution of the corresponding FE results, therefore, suggesting better prediction accuracy over the codified web shear buckling curve of EN1993-1-4 [26]. The mean and COV of proposed EN1993-1-4 [26] provisions given in Table 4 also implies the improved shear resistance predictions for both section types over the current shear provisions.

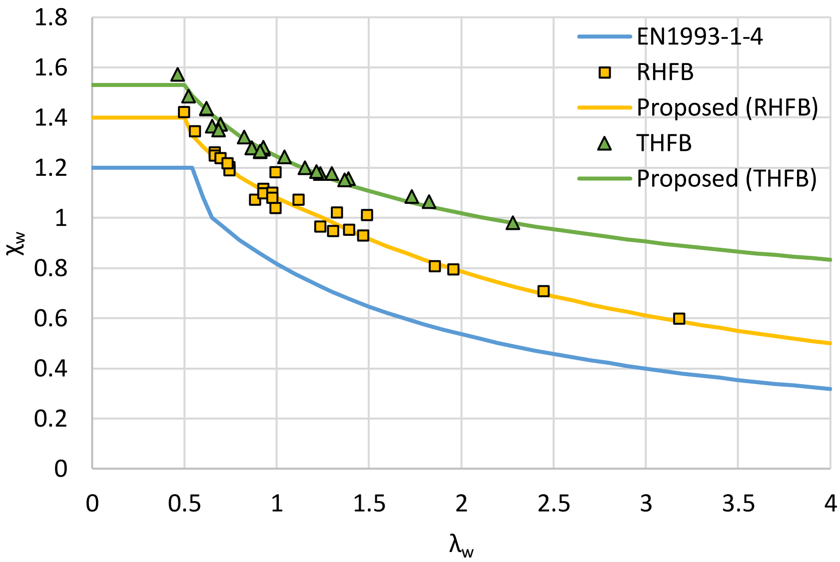

Fig. 10 Comparison of FE shear capacities with the proposed web shear buckling reduction factor (χ_w) for EN1993-1-4 [26]

4.2 The direct strength method

The DSM has been developed as an alternative design approach to the traditional cross-section classification framework known as the effective width method. The clause 7.2.3.3 of Australian and New Zealand standards, AS/NZS 4600 [24] includes the details of the DSM shear design rules for the sections with transverse web stiffeners.

The sectional shear capacity (V_v) according to the DSM is given by Eqs. (14) and (15).

$$V_v = V_y \text{ for } \lambda \leq 0.776 \tag{14}$$

$$V_v = \left[1 - 0.15\left(\frac{1}{\lambda^2}\right)^{0.4}\right]\left(\frac{1}{\lambda^2}\right)^{0.4} V_y \text{ for } \lambda > 0.776 \tag{15}$$

where λ is the cross-sectional slenderness.

The slenderness of the cross-section, λ is defined as in Eq. (16) using the shear yield capacity of the section (V_y) and the elastic shear buckling capacity of the section (V_{cr}).

$$\lambda = \sqrt{\frac{V_y}{V_{cr}}} \tag{16}$$

Eqs. (17) and (18) can be used to calculate the shear yield capacity (V_y) and the elastic shear buckling capacity (V_{cr}) of the section.

$$V_y = 0.6\, f_{yw} d_1 t_w \tag{17}$$

$$V_{cr} = \frac{k\pi^2 E}{12\,(1-\upsilon^2)} \frac{{t_w}^3}{d_1} \tag{18}$$

where f_{yw} is the yield strength of the web, d_1 is the flat depth of the web, t_w is the thickness of the web, E is Young's modulus, υ is Poisson's ratio, and k is the elastic shear buckling coefficient of the section.

The applicability of the DSM shear design provisions to predict the section capacities of cold-formed stainless steel hollow flange sections were then assessed using the numerical parametric study results gathered in Section 3. The elastic shear buckling coefficient (k) of the hollow flange sections were found from Keerthan and Mahendran [22]. Fig. 11 illustrates the FE shear capacities of RHFBs and THFBs together with the DSM shear design curve. Moreover, the overall mean and COV of FE shear capacity to DSM predicted shear capacity ratio for each hollow flange section type is given in Table 4. Both these comparisons reflect that the DSM shear design provisions significantly under-predict the section capacities of stainless steel RHFBs and THFBs as similar to EN1993-1-4 [26] shear design provisions.

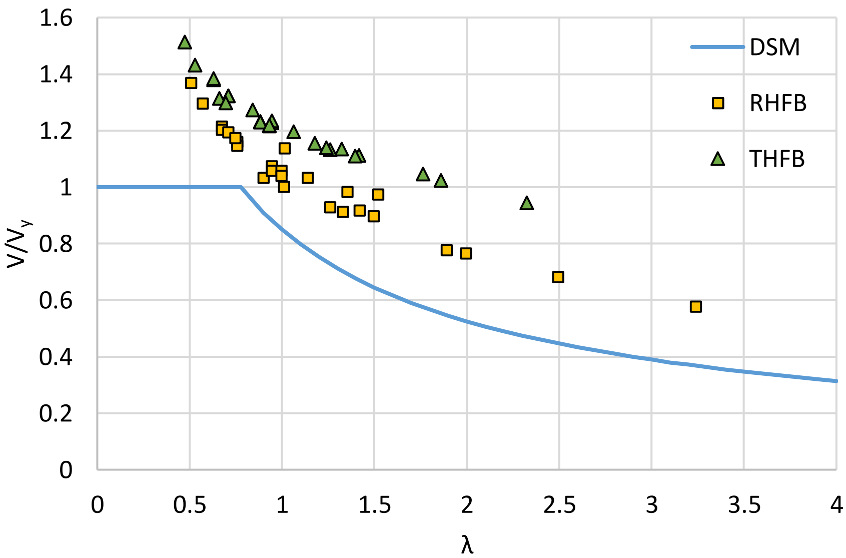

Fig. 11 Comparison of FE shear capacities with the DSM shear design curve

Following the assessment of DSM shear design rules, modifications were made to Eqs. (16) and (17) aiming to achieve improved shear capacity predictions for the cold-formed stainless steel hollow flange sections. Regression analyses were conducted to fit the proposed DSM curves to FE shear capacities.

The proposed DSM equations for stainless steel RHFB sections are expressed in Eqs. (19)-(21).

$$V_v = 1.36V_y \text{ for } \lambda \leq 0.5 \tag{19}$$

$$V_v = \frac{V_y}{\lambda^{0.444}} \text{ for } 0.5 < \lambda \leq 1.0 \tag{20}$$

$$V_v = \left[1 - 0.01\left(\frac{1}{\lambda^2}\right)^{0.232}\right]\left(\frac{1}{\lambda^2}\right)^{0.232} V_y \text{ for } \lambda > 1.0 \tag{21}$$

Eqs. (22) and (23) provide the proposed DSM equations for stainless steel THFB sections.

$$V_v = 1.53V_y \text{ for } \lambda \leq 0.44 \tag{22}$$

$$V_v = \frac{1.206V_y}{\lambda^{0.29}} \text{ for } \lambda > 0.44 \tag{23}$$

The new DSM equations and existing DSM equations for shear are plotted together with the FE capacities of stainless steel RHFBs and THFBs in Fig. 12. The comparison shows that the proposed DSM curves follow the distribution of the respective FE results well. Further, the mean and COV of proposed DSM provisions given in Table 4 suggest enhanced capacity predictions for stainless steel hollow flange sections over the current DSM shear design rules.

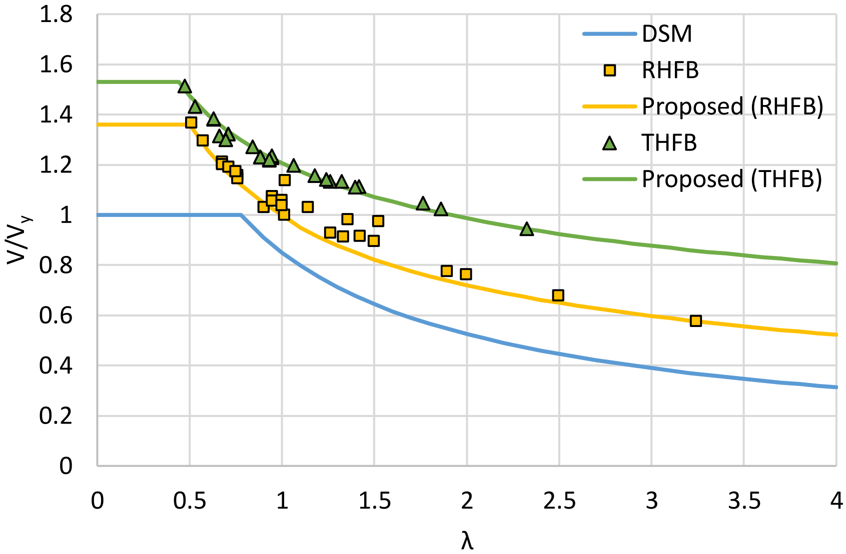

Fig. 12 Comparison of FE shear capacities with the proposed DSM shear design curve

4.3 Reliability analysis

Reliability analysis was conducted for the proposed EN1993-1-4 [26] and the DSM resistance models according to North American specifications for cold-formed steel [23]. The capacity reduction factor ($\emptyset_v$) of each resistance model was calculated using Eq. (24).

$$\emptyset_v = 1.52 M_m F_m P_m e^{-\beta_0 \sqrt{(V_m^2 + V_f^2 + C_p V_p^2 + V_q^2)}} \quad (24)$$

where M_m=1.1 and V_m=0.1 are mean and COV of the material factor, respectively. F_m=1.0 and V_f=0.05 are mean and COV of the fabrication factor, respectively. P_m and V_p (not less than 0.065) are mean and COV of the actual (FE) resistance to predicted resistance ratio, respectively. β_0 is the target reliability index and V_q=0.21 is the COV of the load effect.

The correction factor, C_p is given by Eq. (25).

$$C_p = \left[1 + \frac{1}{n}\right]\left[\frac{m}{m-2}\right] \quad (25)$$

where m=n-1 and n is the total number of data.

For the calculations, the target reliability index, β_0 was taken as 2.5 and the minimum recommended value was assigned for V_p as the actual values were found to be less than 0.065. The calculated capacity reduction factors for the proposed EN1993-1-4 [26] resistance models are 0.91 for RHFBs and 0.90 for THFBs. For the proposed DSM resistance models, the calculated capacity reduction factors are found to be 0.95 for RHFBs and 0.90 for THFBs.

Therefore, a value of 0.90 is recommended in general for the capacity reduction factor of all the resistance functions.

5 Concluding remarks

The shear response of cold-formed stainless steel hollow flange sections was investigated using numerical analysis in this paper. The numerical parametric studies were conducted for RHFB sections and THFB sections using the validated FE models. Various influential parameters such as the height of the section, the thickness of the section and the steel grade were taken into account in the study and 51 FE models of hollow flange sections were developed. The numerical results were used to observe the shear response of the sections and to evaluate the codified shear provisions. From the FE results, it can be observed that diagonal tension fields are formed within section webs of RHFB sections however more even distribution of the stresses can be seen in the webs of THFB sections with no clearly visible tension bands as a result of increased anchoring provided by the flanges. The increased anchoring provided by the flanges results into developing plastic hinge type mechanism in the top flanges of THFB sections at the mid-span. Moreover, the shear resistance of THFBs is found to be relatively higher than RHFBs. In general, the evaluation of EN1993-1-4 [26] and the DSM shear design rules using the generated numerical results suggests that the current codified provisions considerably under-predict the shear resistance of stainless steel hollow flange sections. Therefore, modifications were proposed to the codified provisions aiming improved shear capacity predictions. The proposed shear provisions offer more accurate and consistent shear capacity predictions over the codified provisions. The reliability of the proposed provisions was also assessed.

Acknowledgements

Authors would like to thank Northumbria University for financial support and providing the necessary research facilities to conduct this research.

References

[1] N. R. Baddoo, Stainless steel in construction: A review of research, applications, challenges and opportunities, J. Constr. Steel Res. 64 (11) (2008) pp. 1199–1206.

[2] L. Gardner, Aesthetics, economics and design of stainless steel structures, Adv. Steel Constr. 4 (2) (2008) pp. 113–122.

[3] L. Gardner, The use of stainless steel in structures, Pro. Struct. Eng. Mater. 7 (2) (2005) pp. 45–55.
[4] P. Keerthan, M. Mahendran, Experimental studies on the shear behaviour and strength of LiteSteel beams, Eng. Struct. 32 (10) (2010) pp. 3235–3247.
[5] P. Keerthan, M. Mahendran, New design rules for the shear strength of LiteSteel beams, J. Constr. Steel Res. 67 (6) (2011) pp. 1050–1063.
[6] P. Keerthan, D. Hughes, M. Mahendran, Experimental studies of hollow flange channel beams subject to combined bending and shear actions, Thin-Walled Struct. 77 (2014) pp. 129–140.
[7] P. Keerthan, M. Mahendran, D. Hughes, Numerical studies and design of hollow flange channel beams subject to combined bending and shear actions, Eng. Struct. 75 (2014) pp. 197–212.
[8] R. Siahaan, M. Mahendran, P. Keerthan, Section moment capacity tests of rivet fastened rectangular hollow flange channel beams, J. Constr. Steel Res. 125 (2016) pp. 252–262.
[9] R. Siahaan, P. Keerthan, M. Mahendran, Finite element modeling of rivet fastened rectangular hollow flange channel beams subject to local buckling, Eng. Struct. 126 (2016) pp. 311–327.
[10] K. S. Wanniarachchi, M. Mahendran, Experimental study of the section moment capacity of cold-formed and screw-fastened rectangular hollow flange beams, Thin-Walled Struct. 119 (2017) pp. 499–509.
[11] C. H. Pham, G. J. Hancock, Experimental investigation of high strength cold-formed C-sections in combined bending and shear, J. Struct. Eng. 136 (7) (2010) pp. 866–878.
[12] C. H. Pham, G. J. Hancock, Numerical simulation of high strength cold-formed purlins in combined bending and shear, J. Constr. Steel Res. 66 (10) (2010) pp. 1205–1217.
[13] C. H. Pham, G. J. Hancock, Direct strength design of cold-formed C-sections for shear and combined actions, J. Struct. Eng. 138 (6) (2012) pp. 759–768.
[14] P. Keerthan, M. Mahendran, Experimental investigation and design of lipped channel beams in shear, Thin-Walled Struct. 86 (2015) pp. 174–184.
[15] D. M. M. P. Dissanayake, K. Poologanathan, S. Gunalan, K. D. Tsavdaridis, B. Nagaratnam, K. S. Wanniarachchi, Numerical modelling and shear design rules of stainless steel lipped channel sections, J. Constr. Steel Res. (2019) (In press).
[16] A. Olsson, Stainless steel plasticity-material modelling and structural applications, PhD thesis, Lulea University of Technology, Sweden, 2001.

[17] E. Real, E. Mirambell, I. Estrada, Shear response of stainless steel plate girders, Eng. Struct. 29 (7) (2007) pp. 1626–1640.

[18] N. Saliba, L. Gardner, Experimental study of the shear response of lean duplex stainless steel plate girders, Eng. Struct. 46 (2013) pp. 375–391.

[19] M. Anwar-Us-Saadat, M. Ashraf, The continuous strength method for lateral-torsional buckling of stainless steel I-beams, Thin-Walled Struct. 130 (2018) pp. 148–160.

[20] C. H. Pham, G. J. Hancock, Shear buckling of thin-walled channel sections, J. Constr. Steel Res. 65 (3) (2009) pp. 578–585.

[21] C. H. Pham, G. J. Hancock, Elastic buckling of cold-formed channel sections in shear, Thin-Walled Struct. 61 (2012) pp. 22–26.

[22] P. Keerthan, M. Mahendran, Improved shear design rules of cold-formed steel beams, Eng. Struct. 99 (2015) pp. 603–615.

[23] AISI S100–16, North American Specification for the design of cold-formed steel structural members, American Iron and Steel Institute (AISI), Washington, 2016.

[24] AS/NZS 4600, Cold-formed steel structures, Standards Australia/Standards New Zealand (AS/NZS), Sydney, 2018.

[25] EN 1993-1-3, Eurocode 3 – Design of steel structures – Part 1–3: General rules – Supplementary rules for cold-formed members and sheeting, European Committee for Standardization (CEN), Brussels, 2006.

[26] EN 1993-1-4:2006+A1:2015, Eurocode 3 – Design of steel structures – Part 1–4: General rules – Supplementary rules for stainless steels, European Committee for Standardization (CEN), Brussels, 2015.

[27] O. Zhao, S. Afshan, L. Gardner, Structural response and continuous strength method design of slender stainless steel cross-sections, Eng. Struct. 140 (2017) pp. 14–25.

[28] I. Arrayago, E. Real, L. Gardner, Description of stress-strain curves for stainless steel alloys, Mater. Des. 87 (2015) pp. 540–552.

[29] M. Ashraf, L. Gardner, D. A. Nethercot, Strength enhancement of the corner regions of stainless steel cross-sections, J. Constr. Steel Res. 61 (1) (2005) pp. 37–52.

[30] R. B. Cruise, L. Gardner, Strength enhancements induced during cold forming of stainless steel sections, J. Constr. Steel Res. 64 (11) (2008) pp. 1310–1316.

[31] B. Rossi, S. Afshan, L. Gardner, Strength enhancements in cold-formed structural sections – Part II: Predictive models, J. Constr. Steel Res. 83 (2013) pp. 189–196.

[32] S. Niu, K. J. R. Rasmussen, F. Fan, Distortional-global interaction buckling of stainless steel C-beams: Part II - Numerical study and design, J. Constr. Steel Res. 96 (2014) pp. 40–53.

[33] Y. Liang, O. Zhao, Y. Long, L. Gardner, Stainless steel channel sections under combined compression and minor axis bending – part 1: experimental study and numerical modelling, J. Constr. Steel Res. 152 (2019) pp. 154–161.

[34] L. Gardner, D. A. Nethercot, Numerical modeling of stainless steel structural components–A consistent approach, J. Struct. Eng. 130 (10) (2004) pp. 1586–1601.

[35] M. Ashraf, L. Gardner, D. A. Nethercot, Geometric imperfections in stainless steel cross-sections, Proceedings of the Fourth International Conference on Advances in Steel Structures, 13–15 June 2005, Shanghai, China, pp. 105–112.

[36] M. Ashraf, L. Gardner, D. A. Nethercot, Finite element modelling of structural stainless steel cross-sections, Thin-Walled Struct. 44 (10) (2006) pp. 1048–1062.

[37] R. G. Dawson, A. C. Walker, Post-buckling of geometrically imperfect plates, J. Struct. Div. 98 (1) (1972) pp. 75–94.

[38] EN 1993-1-5, Eurocode 3 – Design of steel structures – Part 1–5: Plated structural elements, European Committee for Standardization (CEN), Brussels, 2006.